Artifact-free reverse time migration

Zhang, Lele; Slob, Evert; van der Neut, Joost; Wapenaar, Kees

DOI
10.1190/GEO2017-0795.1

Publication date
2018

Document Version
Final published version

Published in
Geophysics

GEOPHYSICS, VOL. 83, NO. 5 (SEPTEMBER-OCTOBER 2018); P. A65–A68, 3 FIGS.
10.1190/GEO2017-0795.1

Artifact-free reverse time migration

Lele Zhang[1], Evert Slob[1], Joost van der Neut[1], and Kees Wapenaar[1]

ABSTRACT

We have derived an improved reverse time migration (RTM) scheme to image the medium without artifacts arising from internal multiple reflections. This is based on a revised implementation of Marchenko redatuming using a new time-truncation operator. Because of the new truncation operator, we can use the time-reversed version of the standard wavefield-extrapolation operator as initial estimate for retrieving the upgoing focusing function. Then, the retrieved upgoing focusing function can be used to directly image the medium by correlating it with the standard wavefield-extrapolation operator. This imaging scheme can be seen as an artifact-free RTM scheme with two terms. The first term gives the conventional RTM image with the wrong amplitude and artifacts due to internal multiple reflections. The second term gives a correction image that can be used to correct the amplitude and remove artifacts in the image generated by the first term. We evaluated the success of the method with a 2D numerical example.

INTRODUCTION

Recently, a novel iterative method, called Marchenko imaging, was introduced to retrieve the Green's function with a virtual receiver located in the subsurface of a 3D inhomogeneous medium. This Green's function is obtained from the single-sided reflection response measured at the surface. The development of the single-sided Marchenko scheme has been inspired by Rose (2002), who demonstrates that solving the 1D Marchenko equation can be seen as focusing a wavefield inside the 1D medium. Broggini and Snieder (2012) introduce this to the geophysical field. They find that the 1D focusing function can be combined with its measured, single-sided response to give the 1D Green's function with a virtual receiver at the focal point inside the medium. Wapenaar et al. (2013) derive the theory for 3D media. Slob et al. (2014) use reciprocity relations to create coupled Marchenko equations that can be solved for the up- and downgoing parts of the focusing function. The extension to 3D is given by Wapenaar et al. (2014a), where the obtained focusing function is used for retrieving the Green's function. The retrieved up- and downgoing parts of the Green's function can be used for retrieving the artifact-free image at any focal point (Wapenaar et al., 2014b).

Based on the presented Marchenko scheme, a wide range of applications in the geophysical field have been realized. Meles et al. (2015) combine the Marchenko scheme with seismic interferometry to eliminate internal multiple reflections in the data domain. Singh et al. (2015) extend the scheme to account for free-surface related multiple reflections, such that the free-surface related multiple reflections would not need to be removed before the method can be applied. Ravasi (2017) extends the Marchenko scheme to eliminate free-surface and internal multiple reflections in one step in the marine seismic setting (Slob and Wapenaar, 2017). Van der Neut and Wapenaar (2016) present the projected version of the Marchenko scheme by convolving both sides of the Marchenko equations with the first arrival of the transmission response in the truncated medium. The projected Marchenko scheme avoids the estimation of the first arrival of the downgoing focusing function and can be applied to eliminate internal multiple reflections in the data domain. Wapenaar et al. (2017) derive a scheme for retrieving the homogeneous Green's function between any two points inside a medium from the single-sided reflection response. Although it is derived initially for acoustic wavefield, the Marchenko scheme has been extended to elastic media (da Costa Filho et al., 2014; Wapenaar and Slob, 2014) and to dissipative media (Slob, 2016).

In this paper, we present a revised Marchenko-redatuming scheme by applying a new truncation operator. We show that due to the new truncation operator, the seismic reflection data are redatumed using the first arrival of the downgoing Green's function, which is a standard wavefield extrapolator used for redatuming the sources. Based on this scheme, we derive a migration scheme to image the medium without artifacts arising from internal multiple

Manuscript received by the Editor 7 December 2017; revised manuscript received 3 May 2018; published ahead of production 10 June 2018; published online 2 August 2018.
[1]Delft University of Technology, 2628 CN Delft, The Netherlands. E-mail: l.zhang-1@tudelft.nl; e.c.slob@tudelft.nl; j.r.vanderneut@tudelft.nl; c.p.a.wapenaar@tudelft.nl.

reflections. We show that the first term of this scheme is equal to the conventional reverse time migration (RTM) scheme and the second term gives the correction image, which can be used to correct the amplitude and eliminate artifacts in the conventional RTM image. Hence, the second term can also be used to correct an existing RTM image when the same data set and macromodel are available. We give a 2D numerical example to illustrate the performance of the proposed method.

METHOD

We indicate time as t and the position vector of a spatial coordinate as $\mathbf{x} = (x, y, z)$, where z denotes the depth and (x, y) denote the horizontal coordinates. An acoustically transparent acquisition boundary $\partial\mathbf{D}_0$ is defined at $z_0 = 0$. For convenience, the coordinates at $\partial\mathbf{D}_0$ are denoted as $\mathbf{x}_0 = (\mathbf{x}_H, z_0)$, with $\mathbf{x}_H = (x, y)$. Similarly, the position vector of a point at an arbitrary depth level $\partial\mathbf{D}_i$ is denoted as $\mathbf{x}_i = (\mathbf{x}_H, z_i)$, where z_i denotes the depth of $\partial\mathbf{D}_i$. We express the acoustic impulse reflection response as $R(\mathbf{x}'_0, \mathbf{x}_0, t)$, where $\mathbf{x}_0$ denotes the source position and $\mathbf{x}'_0$ denotes the receiver position, both located at the acquisition surface $\partial\mathbf{D}_0$. In practice when using field-measured data, this means that first free-surface related multiple reflections should be removed from the measured reflection response. Assuming that sources are above the receiver array, source locations should be redatumed to the receiver depth level and the source wavelet should be estimated. The focusing function $f_1(\mathbf{x}_0, \mathbf{x}_i, t)$ is the solution of the homogeneous wave equation in a truncated medium and focuses at the focal point $\mathbf{x}_i$. We define the truncated domain as $z_0 < z < z_i$. Inside the truncated domain, the properties of the medium are equal to the properties of the physical medium. Outside the truncated domain, the truncated medium is reflection free. The Green's function $G(\mathbf{x}_i, \mathbf{x}_0, t)$ is defined for an impulsive source that is excited at $\mathbf{x}_0$, and a receiver is positioned at the focal point $\mathbf{x}_i$. The Green's function is defined in the same physical medium as the measured data. The focusing and Green's functions can be partitioned into up- and downgoing parts, and, for this, we use power-flux normalized quantities (Wapenaar et al., 2014a).

We start with the 3D versions of one-way reciprocity theorems for flux-normalized wavefields and use them for the depth levels z_0 and z_i. When the medium above the acquisition level z_0 is reflection free, the Green's function representations are given by (Wapenaar et al., 2014a)

$$G^-(\mathbf{x}_i,\mathbf{x}'_0,t) = \int_{\partial\mathbf{D}_0} d\mathbf{x}_0 \int_0^{+\infty} R(\mathbf{x}'_0,\mathbf{x}_0,t') f_1^+(\mathbf{x}_0,\mathbf{x}_i,t-t')dt' - f_1^-(\mathbf{x}'_0,\mathbf{x}_i,t), \quad (1)$$

$$G^+(\mathbf{x}_i,\mathbf{x}'_0,-t) = -\int_{\partial\mathbf{D}_0} d\mathbf{x}_0 \int_{-\infty}^0 R(\mathbf{x}'_0,\mathbf{x}_0,-t') f_1^-(\mathbf{x}_0,\mathbf{x}_i,t-t')dt' + f_1^+(\mathbf{x}'_0,\mathbf{x}_i,t). \quad (2)$$

Superscripts $+$ and $-$ stand for the downgoing and upgoing parts, respectively. We write the downgoing Green's function as the sum of a direct part and a coda:

$$G^+(\mathbf{x}_i, \mathbf{x}_0, t) = G_d^+(\mathbf{x}_i, \mathbf{x}_0, t) + G_m^+(\mathbf{x}_i, \mathbf{x}_0, t), \quad (3)$$

where G_d^+ indicates the direct part and G_m^+ the following coda. As explained in Wapenaar et al. (2014a), the Green's and focusing functions in equations 1 and 2 are separated in time except for the first event in f_1^+ and the last event in $G^+(-t)$ in equation 2 that coincide with each other. We rewrite equations 1 and 2 with the help of equation 3 as

$$f_1^-(\mathbf{x}'_0,\mathbf{x}_i,t) = \int_{\partial\mathbf{D}_0} d\mathbf{x}_0 \int_0^{+\infty} R(\mathbf{x}'_0,\mathbf{x}_0,t') f_1^+(\mathbf{x}_0,\mathbf{x}_i,t-t')dt', \quad \text{for } -t_d-\varepsilon<t<t_d+\varepsilon, \quad (4)$$

$$f_1^+(\mathbf{x}'_0,\mathbf{x}_i,t) - G_d^+(\mathbf{x}_i,\mathbf{x}'_0,-t) = \int_{\partial\mathbf{D}_0} d\mathbf{x}_0 \int_{-\infty}^0 R(\mathbf{x}'_0,\mathbf{x}_0,-t') f_1^-(\mathbf{x}_0,\mathbf{x}_i,t-t')dt', \quad \text{for } -t_d-\varepsilon<t<t_d+\varepsilon, \quad (5)$$

where t_d denotes the one-way traveltime from a surface point $\mathbf{x}'_0$ to the focusing point $\mathbf{x}_i$ and ε is a positive value to account for the finite bandwidth. Note that the truncation interval is longer in equations 4 and 5 than in the conventional Marchenko scheme $(-t_d + \varepsilon < t < t_d - \varepsilon)$. The left extension of the truncation interval ensures that the time-reversed G_d^+ is present in equation 5, whereas it is excluded in the conventional Marchenko scheme (Wapenaar et al., 2014a). The right extension of the truncation interval ensures that when the focusing point is just above a reflector, the reflection of that reflector is the last event in f_1^-, whereas this reflection would be the first event in G^- in the scheme of Wapenaar et al. (2014a). We give equations 4 and 5 in operator form as

$$f_1^-(\mathbf{x}'_0,\mathbf{x}_i,t) = [\Theta\mathbf{R}f_1^+](\mathbf{x}'_0,\mathbf{x}_i,t), \quad (6)$$

$$f_1^+(\mathbf{x}'_0,\mathbf{x}_i,t) = [\Theta\mathbf{R}^* f_1^- + G_d^{+*}](\mathbf{x}'_0,\mathbf{x}_i,t), \quad (7)$$

where G_d^{+*} indicates the time-reversed version of G_d^+, $\mathbf{R}$ indicates an integral operator of the measured data R with any wavefield as in equation 4, $\mathbf{R}^*$ a similar correlation integral operator as in equation 5, and Θ is a time window to exclude values outside the interval $(-t_d - \varepsilon, t_d + \varepsilon)$ as indicated by the time window in equations 4 and 5. Then, we substitute equation 7 into equation 6 to get the final equation for f_1^- as

$$[(I - \Theta\mathbf{R}\Theta\mathbf{R}^*)f_1^-](\mathbf{x}'_0,\mathbf{x}_i,t) = [\Theta\mathbf{R}G_d^{+*}](\mathbf{x}'_0,\mathbf{x}_i,t). \quad (8)$$

We expand equation 8 as a Neumann series to give the equation as

$$f_1^-(\mathbf{x}'_0,\mathbf{x}_i,t) = [\Theta\mathbf{R}G_d^{+*}](\mathbf{x}'_0,\mathbf{x}_i,t) + \left[\sum_{m=1}^{\infty}(\Theta\mathbf{R}\Theta\mathbf{R}^*)^m\Theta\mathbf{R}G_d^{+*}\right](\mathbf{x}'_0,\mathbf{x}_i,t). \quad (9)$$

The first term in the right side of equation 9 is the reflection response redatumed to the subsurface point $\mathbf{x}_i$ by the redatuming operator G_d^+. It is truncated to make sure the result is set to zero for $t > t_d$. The

second term in the right side of equation 9 predicts and removes multiple reflections that occur in the reflection data in the time window. It thereby removes the transmission effects of the primary reflections between the acquisition plane and the depth level of the focusing point. When the focal point coincides with an actual subsurface reflector, its primary reflection will occur in f_1^- at time instant t_d. Otherwise, the value in f_1^- at that time instant will be zero. For each pair of points in the left side of equation 9, we are interested only in the value of f_1^- at time instant t_d. By carrying out downward extrapolation at the receiver side, we create the image at the focal point. Correlating both sides of equation 9 with G_d^+ gives

$$\mathbf{I}(\mathbf{x}_i,\mathbf{x}_i,t) = \left[\mathbf{G}_d^{+*}\mathbf{R}G_d^{+*}+\mathbf{G}_d^{+*}\sum_{m=1}^{\infty}(\Theta\mathbf{R}\Theta\mathbf{R}^*)^m\Theta\mathbf{R}G_d^{+*}\right](\mathbf{x}_i,\mathbf{x}_i,t), \quad (10)$$

with $\mathbf{I}(\mathbf{x}_i,\mathbf{x}_i,t)$ defined as the space-time image function and $\mathbf{G}_d^{+*}$ indicates a correlation integral operator of G_d^+ with any wavefield. The possible primary reflection of interest in f_1^- at t_d occurs at $t = 0$ after the downward extrapolation. We can now understand that the image function $\mathbf{I}(\mathbf{x}_i,\mathbf{x}_i,t)$ can be used for estimating the artifact-free image of the point $\mathbf{x}_i$ at $t = 0$. The first term in the right side of equation 10 can be understood as the conventional RTM scheme. It produces the conventional RTM image of the point $\mathbf{x}_i$ at $t = 0$, in which artifacts due to internal multiple reflections can be present. Consequently, the second term in the right side of equation 10 can be seen as an operator expression for correcting the amplitude of the primary reflections and for removing artifacts contained in the conventional RTM image. It uses only the single-sided reflection response and simple time truncations together with the same information needed to construct a conventional RTM image. The scheme easily fits in routine RTM migration operations. We state that equation 10 presents an improved RTM scheme that can be used for retrieving the artifact-free image of the subsurface.

EXAMPLE

The aim of the current method is to image the medium without artifacts arising from internal multiple reflections and without using more information than in standard migration schemes. To illustrate the method, we give a 2D numerical example. Figure 1a shows the values for the acoustic velocity as a function of depth and horizontal position. Figure 1b shows the smoothed velocity model that will be used to do the conventional and artifact-free RTM. The source emits a Ricker wavelet with a 20 Hz center frequency. We have computed the single-sided reflection responses with 601 sources and 601 receivers on a fixed spread with spacing of 10m at the top of the model. Absorbing boundary conditions are applied around the model, and the direct wave has been removed. One of the computed single-sided reflection responses convolved with the source wavelet is shown in Figure 2a. Note that internal multiple reflections occur at later times. First arrivals of the downgoing Green's functions have been modeled based on the smoothed model shown in Figure 1b with sources at focal points and receivers at the acquisition surface. One of the computed first arrivals convolved with the source wavelet is shown in Figure 2b. The computed single-sided reflection responses and time-reversed first arrivals are used as inputs to solve equation 10 with $m = 1, \ldots, 20$. The resulting artifact-free image of the target zone is shown in Figure 3a. Then,

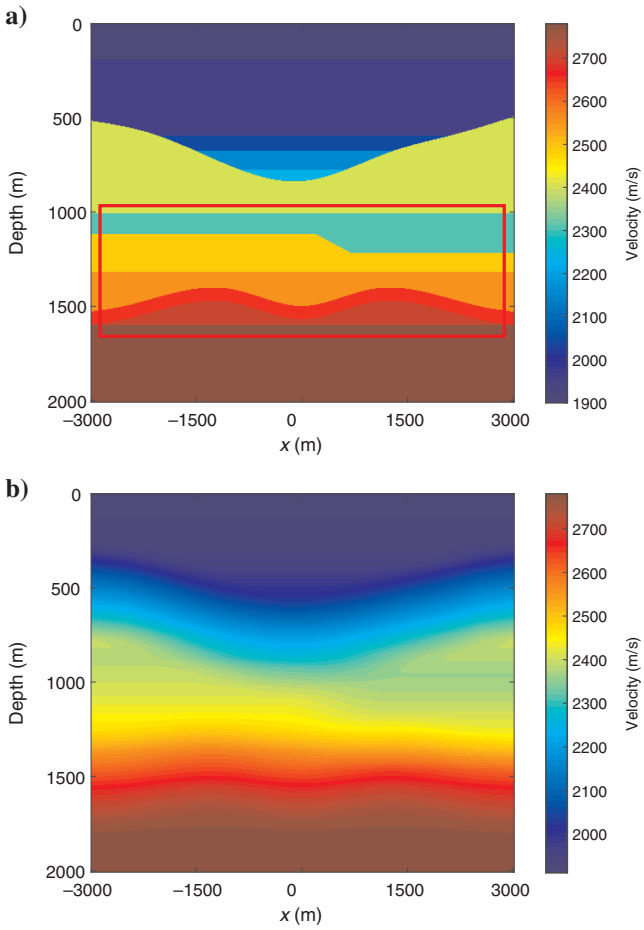

Figure 1. (a) Velocity model that will be used to model the reflection response, and the red box gives the target zone that will be imaged. (b) The smoothed velocity model that will be used to model the first arrival of the downgoing Green's function.

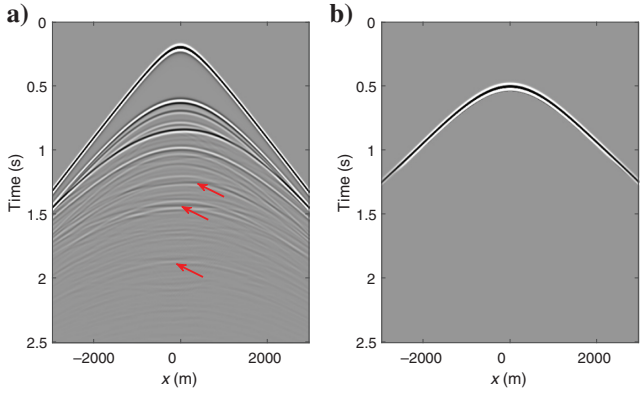

Figure 2. (a) The modeled reflection response with source and receivers at the acquisition surface. The red arrows indicate the internal multiple reflections. (b) The modeled first arrival of the downgoing Green's function with source at the focal point in the subsurface and receivers at the acquisition surface.

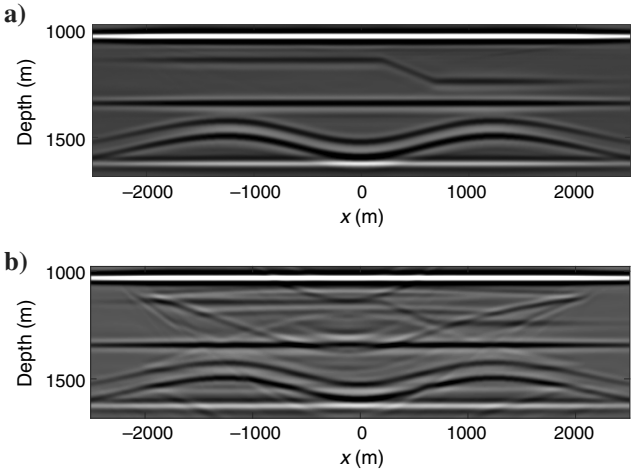

Figure 3. (a) The artifact-free image of the target zone retrieved in equation 10. (b) The image of the target zone retrieved by the first term in the right side of equation 10.

the procedure as described using the first term in the right side of equation 10 is applied and leads to the conventional RTM image of the target zone shown in Figure 3b. Note that Figure 3b contains artifacts from internal multiple reflections because they are imaged as if they were primary reflections. However, the image in Figure 3a obtained with the new scheme is nearly perfect without ghost images due to internal multiple reflections. For both images, the smoothed velocity model shown in Figure 1b was used and the two figures can be compared as best-case scenarios.

In the derivation of the current method, we assumed the medium to be lossless. The method can be adapted to work with two-sided reflection and transmission data in dissipative media (Slob, 2016). We further assumed that the Green's functions and the focusing functions can be separated in time and that the source wavelet can be well-recovered, and we ignored evanescent waves (Wapenaar et al., 2013). These restrictions limit the application of the current method. For situations in which these assumptions are fulfilled, the 2D numerical example illustrates that the current method has good potential for applying it to field data. Applicability to field data requires properly sampled data this condition can be fulfilled in 2D, but it is not fulfilled in 3D data acquisition, and modifications will be necessary before the method can work on 3D data.

CONCLUSION

We have shown that an artifact-free RTM image can be constructed based on a revised Marchenko scheme. The revised Marchenko redatuming is applied using a new truncation operator and a time-reversed version of the standard wavefield-extrapolation operator as initial estimate. Based on this, we derived an artifact-free RTM scheme that can be used to image the medium without artifacts arising from internal multiple reflections. The new migration scheme uses the same macrovelocity model as the conventional RTM scheme. The constructed image does not contain artifacts because the data act as an operator to remove artifacts generated by the conventional RTM scheme. When the velocity model is accurate, the image is nearly perfect as shown with a numerical example.

ACKNOWLEDGMENTS

This work is part of the Open Technology Program with project number 13939, which is financed by NWO Domain Applied and Engineering Sciences. We would like to thank J. Blanch, F. Broggini, and an anonymous reviewer for their valuable suggestions. The 2D reflection response in this letter is generated with the finite-difference package in Thorbecke and Draganov (2011).

REFERENCES

Broggini, F., and R. Snieder, 2012, Connection of scattering principles: A visual and mathematical tour: European Journal of Physics, **33**, 593–613, doi: 10.1088/0143-0807/33/3/593.

da Costa Filho, C. A., M. Ravasi, A. Curtis, and G. A. Meles, 2014, Elastodynamic Green's function retrieval through single-sided Marchenko inverse scattering: Physical Review E, **90**, 063201, doi: 10.1103/PhysRevE.90.063201.

Meles, G. A., K. Löer, M. Ravais, A. Curtis, and C. A. da Costa Filho, 2015, Internal multiple prediction and removal using Marchenko autofocusing and seismic interferometry: Geophysics, **80**, no. 1, A7–A11, doi: 10.1190/geo2014-0408.1.

Ravasi, M., 2017, Rayleigh-Marchenko redatuming for target-oriented, true-amplitude imaging: Geophysics, **82**, no. 6, S439–S452, doi: 10.1190/geo2017-0262.1.

Rose, J. H., 2002, Single-sided autofocusing of sound in layered materials: Inverse Problems, **18**, 1923–1934, doi: 10.1088/0266-5611/18/6/329.

Singh, S., R. Snieder, J. Behura, J. van der Neut, K. Wapenaar, and E. Slob, 2015, Marchenko imaging: Imaging with primaries, internal multiples, and free-surface multiples: Geophysics, **80**, no. 5, S165–S174, doi: 10.1190/geo2014-0494.1.

Slob, E., 2016, Green's function retrieval and Marchenko imaging in a dissipative acoustic medium: Physical Review Letters, **116**, 164301, doi: 10.1103/PhysRevLett.116.164301.

Slob, E., and K. Wapenaar, 2017, Theory for Marchenko imaging of marine seismic data with free surface multiple elimination: 79th Annual International Conference and Exhibition, EAGE, Extended Abstracts, doi: 10.3997/2214-4609.201700800.

Slob, E., K. Wapenaar, F. Broggini, and R. Snieder, 2014, Seismic reflector imaging using internal multiples with Marchenko-type equations: Geophysics, **79**, no. 2, S63–S76, doi: 10.1190/geo2013-0095.1.

Thorbecke, J. W., and D. Draganov, 2011, Finite-difference modeling experiments for seismic interferometry: Geophysics, **76**, no. 6, H1–H18, doi: 10.1190/geo2010-0039.1.

Van der Neut, J., and K. Wapenaar, 2016, Adaptive overburden elimination with the multidimensional Marchenko equation: Geophysics, **81**, no. 5, T265–T284, doi: 10.1190/geo2016-0024.1.

Wapenaar, K., F. Broggini, E. Slob, and R. Snieder, 2013, Three dimensional single-sided Marchenko inverse scattering, data-driven focusing, Green's function retrieval, and their mutual relations: Physical Review Letters, **110**, 084301, doi: 10.1103/PhysRevLett.110.084301.

Wapenaar, K., and E. Slob, 2014, On the Marchenko equation for multicomponent single-sided reflection data: Geophysical Journal International, **199**, 1367–1371, doi: 10.1093/gji/ggu313.

Wapenaar, K., J. Thorbecke, J. van der Neut, F. Broggini, E. Slob, and R. Snieder, 2014a, Green's function retrieval from reflection data, in absence of a receiver at the virtual source position: Journal of the Acoustical Society of America, **135**, 2847–2861, doi: 10.1121/1.4869083.

Wapenaar, K., J. Thorbecke, J. van der Neut, F. Broggini, E. Slob, and R. Snieder, 2014b, Marchenko imaging: Geophysics, **79**, no. 3, WA39–WA57, doi: 10.1190/geo2013-0302.1.

Wapenaar, K., J. Thorbecke, J. van der Neut, E. Slob, and R. Snieder, 2017, Virtual sources and their responses. Part II: Data-driven single-sided focusing: Geophysical Prospecting, **65**, 1430–1451, doi: 10.1111/1365-2478.12495.